

Original Article

Signaling Relay Contact Failure Analysis with 3D Profilometry, SEM and EDS

Susmita Sau¹, Sajjan Kumar², Sankar Narayan Patra³, Subhash Chandra Panja⁴

^{1,4}Department of Mechanical Engineering, Jadavpur University, West Bengal, India.

²Department of Electrical and Electronics Engineering, Sri Sivasubramaniya Nadar College of Engineering, Tamil Nadu, India.

³Department of Instrumentation and Electronics Engineering, Jadavpur University, West Bengal, India.

¹Corresponding Author : susmita.sau@gmail.com

Received: 15 October 2023

Revised: 20 November 2023

Accepted: 12 December 2023

Published: 20 January 2024

Abstract - Electromagnetic relays may fail after long-term usage, which is a regular incident. Electromagnetic relay plays a vital role in the interlocking of railway signalling systems. To run the train in fail-safe conditions, signalling components have to work correctly. The signalling relay is an empirical part of the signalling system. Silver-Impregnated Graphite (SIG) contacts are commonly used in the metal to carbon contact relay. Contact resistance becomes high. Disintegration of the contact surface occurs due to erosive wear. A thin film of sulphide and oxide is formed on it due to environmental stress, such as moistness, weather, oxidizing agents, etc. This paper deals with the contact failure analysis of both QN1 series relay contacts. Surface roughness analysis was done through 3D profilometry for both used and unused contacts. Roughness parameters have been calculated. SEM, EDS, and FESEM investigate silver-permeated graphite contact. Surface analysis of SIG contact involves employing SEM to examine the film deposition process, enabling thorough examination of surface attributes. The molecular components of this micro-coating have been investigated by using energy EDS for both SIG contact and silver contact. Oxide, carbide, and sulphide thin coating were identified. High-resolution images of the surface captured by FESEM and SEM feature roughness and a porous structure due to oxidation, sulphation, and corrosion of the contact surface. The investigation of relay contacts prior to thin layer development and successive to high contact resistance indicates that the persistent operation of QN1 series relays culminates in mechanical weakening and transformation, ultimately leading to relay malfunction.

Keywords - Signalling relay, Failure analysis, Roughness analysis, Scanning Electron Microscopy, Energy dispersive X-Ray spectroscopy, Field Emission Scanning Electron Microscopy.

1. Introduction

Electromagnetic relay serves as a crucial circuit breaker for diverse applications such as railway signalling systems, aerospace, electric vehicles, military, smart grids, hybrid electric vehicles, etc. [1]. Relay failures can result in electronic/electrical device malfunctions. The relay's reliability significantly affects the overall dependability of the electrical system. Roughly 70% of relay failures stem from contact issues [2].

Railway signalling relays are used for high-safety purposes. Electromagnetic relays function under varied conditions, each with unique variables like temperature, storage, dust, transport, humidity, and vibration. Ion deposition in the contact surface over many years results in ageing. Temperature fluctuations influence relay parameters and can lead to elevated contact resistance. In addition to that, humidity is one of the factors of surface oxidation that leads to contact corrosion; another contaminant present on the

surface causes sulphation, carbide formation, and contact resistance to be significantly high, and the relay failed [3].

The integration of electromagnetic relays is essential within railway signalling systems. These relays in railway signalling are grouped by various types, such as mounting on plug board, AC-DC supply, contact types (metal or carbon), and line and track relays. Factors like atmosphere, overuse, and improper contact can lead to material failure and deviation from intended logic.

The failure of metal-to-carbon relays may cause significant economic loss for railway transportation organizations. In this context, it is of utmost need to study and analyze the operating behaviour and failure pattern of the relay to maximize its reliability [4].

The reasons related to this electromechanical relay failure can be categorized as follows [5]:



- Different external reasons, such as discontinuous power supply, defective wearing or blowing-off of fuses, and
- Various internal reasons, such as manufacturing defects, poor component quality and malfunctioning of relay components.

Apart from the reasons mentioned above, there are several other causes like high contact resistance, coil breakage, coil burning, foreign matter interference, sulphation of springs/connectors, breakage of an armature, relay cover, and slipping of retaining clips [6, 7] which are reported for analysing performance in modern maintenance technologies and practices, to find potential risks of unexpected failures in a relay. Any deficiencies in the relay manufacturing process result in instant failure when installed in the circuit. All these kinds of failures suggest the need for a reliability analysis of the product outcome [8].

In continuation of this, the high contact resistance developed in the Silver-Impregnated Graphite (SIG) contact [3] seems to be one of the reasons for the poor reliability of metal-to-carbon relays. A thin film layer of oxide and sulphide may also be found on the Silver-Impregnated Graphite (SIG) contact.

A detail of surface topography inspection based on SEM analysis of failed relays of the SIG contact gradually becomes an important research area of interest. In another application, the relay within military weapon systems is subject to thorough scrutiny and evaluation examination [9].

The decomposition of these systems causes the gradual buildup of polluting agents on contact surfaces, ultimately leading to relay failures [10]. Contact adhesion arises from the erosion of the coated contact material, leading to an increase in contact resistance and ultimately causing relay failures. Furthermore, contact adhesion has a significant impact on the lifespan of electromechanical relays [11, 12].

In another research work, in order to evaluate relay reliability, testing involves applying various loads using capacitors, subjecting them to varying current levels across numerous cycles to assess relay reliability [13-15]. Therefore, to better understand the structural changes in movable and fixed contacts, a degradation model was used to simulate the relay in this research [16, 17]. The experiment was conducted with 1000 and 6000 cycles. Demonstrate the involvement of polymer decomposition, which plays a role in arc erosion. This arc reaction led to the formation of oxide contaminations, with the detection of phosphorous on the contact surface [18, 19].

Furthermore, contact surface erosion was observed during stress and the formation of a molten arc. To combat corrosion and prolong contact lifespan, a thin coating with

solid or semi-solid lubricants of carbon allotropes can be applied. Additionally, the use of composite and layered materials can help mitigate damage to the contact interface [20-22].

The examination involved graphene-coated contacts with various coating depths, comparing their effects to those of different thin-layer coatings using finite element analysis. To prevent relay failures, careful selection of contact materials is crucial, aiming for elements that enhance lifespan and withstand adverse atmospheric conditions.

Therefore, evaluating contact surfaces is essential. FESEM is a valuable tool for inspecting cell and material surfaces, particularly for detecting mechanical deformation on relay contact surfaces [23, 24]. EDS identifies the distribution of chemical contaminants on contact interfaces, with energy distribution revealing the mass concentration of surface atoms [25].

In another context, surface roughness parameters analysis using a profilometer is a practical approach. Various techniques encompass visual evaluation, SEM, profilometer, laser, specular reflectance, and AFM [26, 27].

A comparative approach between SEM and profilometer has been taken. The objective was to assess the efficacy and practical applicability of indirect method for characterizing surface topography. SEM images visually describe subjective information about the surface topology, but profilometry showed better results for high dispersion. Profilometry proves to be a valuable and efficient tool compared to other analyses [28].

In this proposed work, a novel methodology has been applied to an electromechanical railway signalling relay with metal-to-carbon contact. As discussed, the resistance of the contact surface became high after thousands of switching operations. The operating contact resistance of the QN1 series relay is less than two hundred milliohms. After thousands of operations, contact resistance becomes more significant than two hundred mili-ohms, and safety issues arise for train movement.

Previous research work focused on the contact resistance of the relay contact, which had increased and reliability is poor. However, surface failure analysis has not been done. Here, a detailed failure analysis has been done in this proposed work. Reduction reaction and oxidation occurred on the metal-to-carbon surface.

A similar kind of work has been done using regular electrical relays and aerospace relays. However, the proposed methodology has been applied to the QN1 series relay with sixteen different types of contacts.

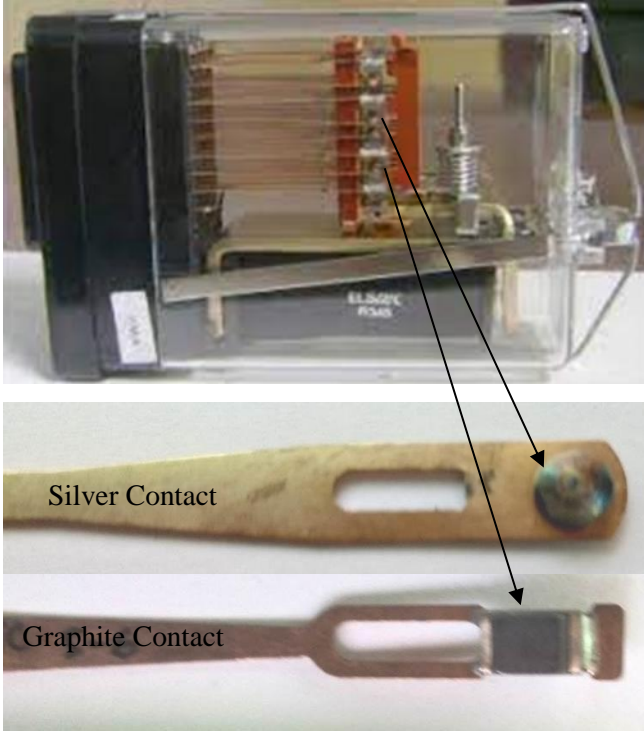


Fig. 1 QN1 series signalling relay and relay contacts dismantled SIG contact and silver contact

Table 1. Factors for relay failure

Cause of Relay Failure	Percentage of Failure
High Contact Resistance	85
Coil Defect	5
Holding Clip Broken	5
Others	5

The metal-to-carbon contact relay has a graphite contact, which is a movable contact, and a silver contact, which is a fixed contact. Graphite contact is a softer material than silver contact; for that reason, mechanical damage occurs on the surface of the contact surface.

Hence, there are other reasons for the mechanical damage on the surface that was previously mentioned. Surface roughness was analysed using 3D profilometry. The roughness of the surface of the relay maximizes after certain mechanical damages.

Moveable graphite contact roughness parameters have been analysed under varying circumstances. As the contact resistance became high, the relay failed. A thin film layer of oxide and sulphide may also be found on the Silver-Impregnated Graphite (SIG) contact previously mentioned.

A detailed surface topography inspection based on SEM analysis of failed relays of the SIG contact and silver contacts

are the research objectives of the proposed work. Therefore, the graphite contact surface is examined preceding and succeeding failure to find the reasons for relay contact failure. FESEM and SEM analyses were done on the graphite contact surfaces.

EDS was also performed on the silver contact and graphite contact pre-failure and post-failure to find the chemical distribution of elements on the surface. From January 2016 to April 2016, South-Eastern Railway faced multiple relay failures, and the corresponding factors of relay failure data are shown in Table 1.

2. Materials and Methods

A signalling relay with a carbon contact relay is used here. Metal-to-carbon contact relays are used in various signalling circuits. These relays have silver and silver-impregnated graphite (carbon).

The make-and-break sequences mimic various choices within signalling circuits. The signalling relay consists of contacts, coil, and spring. Here, we have used a QN1 series plug-in type relay in this work. QN1 series signalling relay and its dismantled SIG contact and silver contact are shown in Figure 1. It has eight front contacts and eight back contacts. The operating voltage is 24V relays.

Pickup time is 150 ms and discharge time is 20 ms. Operating current 60mA, Maximum pickup voltage 19.2 V and DA volts 3.6V. Before the failure, the contact surface was smooth and free from irregularities, but after the failure, a detailed analysis was done for both contacts.

2.1. Surface Topography Analysis

In this research, a plug-in type signalling relay with a carbon contact relay is used for surface anatomy analysis. Roughness parameters have been analysed using 3D profilometry.

The graphite contact surface roughness parameter has been analysed before the knocking condition and after ten thousand knocking conditions in 2D and 3D dimensions.

Therefore, arithmetic average roughness (Ra), R.M.S average roughness (Rq), maximum profile peak height (Rp), maximum profile depth (Rv), sum of the maximum peak height and maximum profile depth (Rt) has been calculated using the formulas below.

$$Ra = 1/l \int_0^l |y(x)| dx \tag{1}$$

$$Rq = \sqrt{\frac{1}{l} \int_0^l \{y(x)\}^2 dx} \tag{2}$$

$$Rp = \max(y_{pi}) \tag{3}$$

$$Rt = \max(y_{pi}) + \max(y_{vi}) \quad (4)$$

$$Rv = \max(y_{vi}) \quad (5)$$

Hence, in more detail, anatomy has been analysed through FESEM and SEM, providing high-resolution magnifications. Graphite contact has been examined, preceding and succeeding failures in various magnified images. EDS has investigated fixed silver and graphite contact preceding and succeeding failure conditions. EDS was performed to find the chemical content of the elements present on the contact interface.

3. Results and Discussion

The performance of the contact interface was observed at different conditions of relay contact failure. Section 3.1 deliberates the performance of the SIG contact pre-failure and the post-failure conditions. In the study of failures, movable SIG contact was considered because SIG contact material is softer than fixed silver contact. SIG and silver contacts of the relay preceding and ensuing failure states are examined separately, and outcomes are explored intricately in Section 4.

3.1. Analysis of SIG Contact Failure

The contacts were examined intricately to investigate the malfunction of the QN1 series relay. A relay ahead of breakdown has been considered here. A SIG contact surface roughness has been tested via 3D profilometry and surface topography using FESEM, SEM, and EDS at pre and post-failure conditions.

3.1.1. Roughness Analysis

SIG contact surfaces with dimensions of length 4.7 mm and width 4.5 mm have been investigated through a 3D optical surface profiler manufactured by Bruker surface roughness before knocking condition. Figure 2, and Figure 4 show the 2D surface roughness of the SIG contact before failure, as well as Figure 3, and Figure 5 shows 3D surface roughness of the SIG contact before failure. One another SIG contact has investigated after ten thousand of knocking failed condition.

Figure 6 shows the 2D surface roughness of failed SIG contact, and Figure 7 shows 3D surface roughness after 10,000 knockings of SIG contact. Figure 8 shows the 2D surface roughness of SIG contact under post-failure conditions, and Figure 9 shows the 3D surface roughness of SIG contact under post-failure conditions after 15,000 knocking.

The surface roughness parameter was measured before the knocking of SIG contact, and the surface roughness parameters after 10,000 and 15,000 knockings are shown in Table 6. And Table 7 arithmetic average roughness (Ra), RMS average roughness (Rq), maximum profile peak height (Rp), maximum profile depth (Rv), sum of the maximum Peak height and maximum profile depth (Rt) has been calculated.

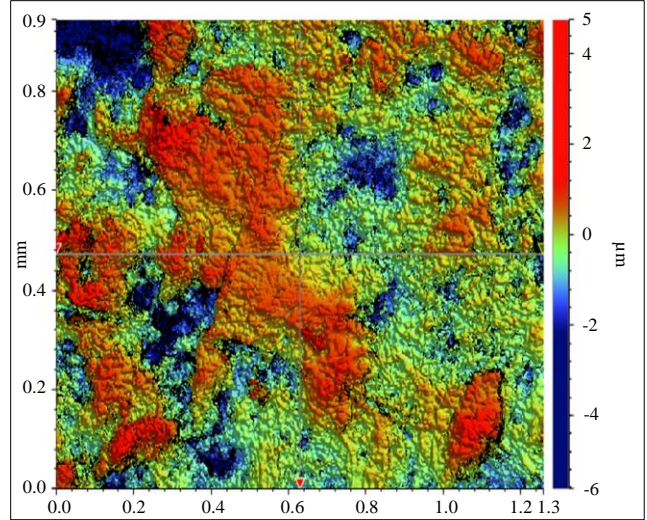


Fig. 2 Surface roughness of SIG contact before knocking (2D-sample 1)

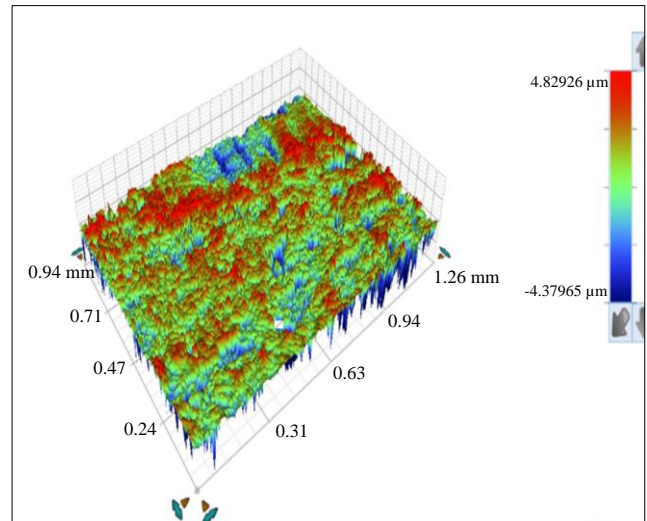


Fig. 3 Surface roughness of SIG contact before knocking (3D-sample 1)

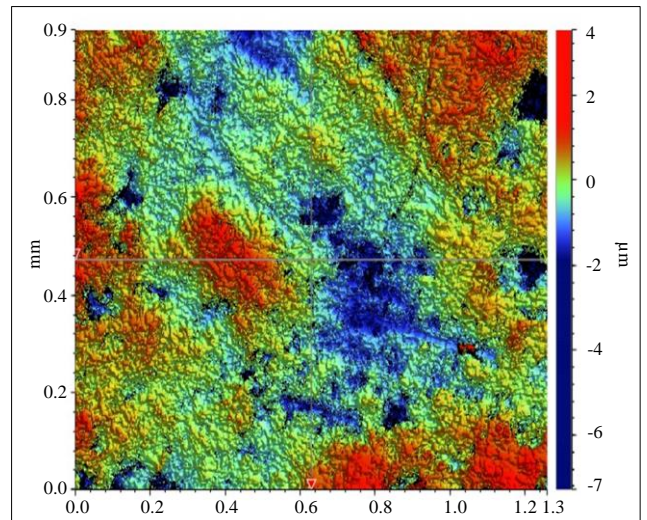


Fig. 4 Surface roughness of SIG contact before knocking (2D-sample 2)

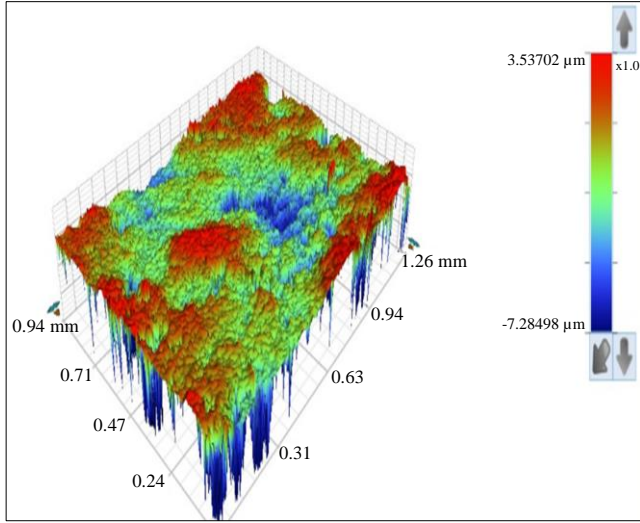


Fig. 5 Surface roughness of SIG contact before knocking (3D-sample 2)

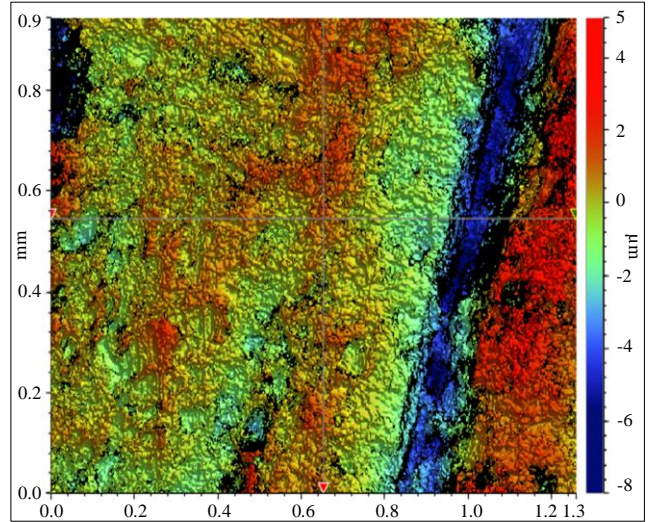


Fig. 8 Surface roughness of SIG contact post-failure (2D-sample 4)

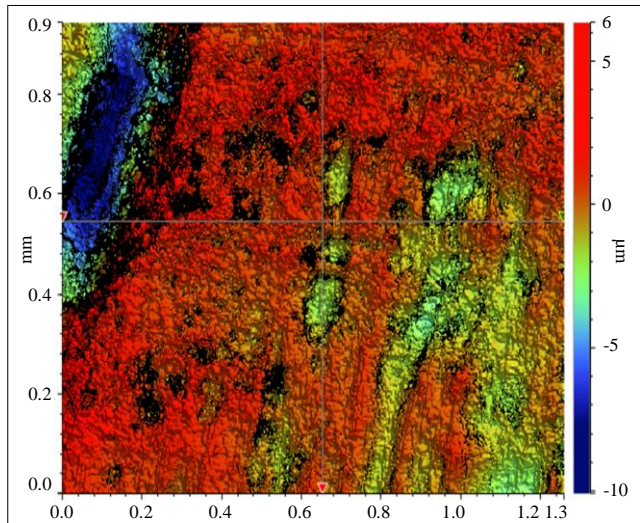


Fig. 6 Surface roughness of SIG contact post-failure (2D-sample 3)

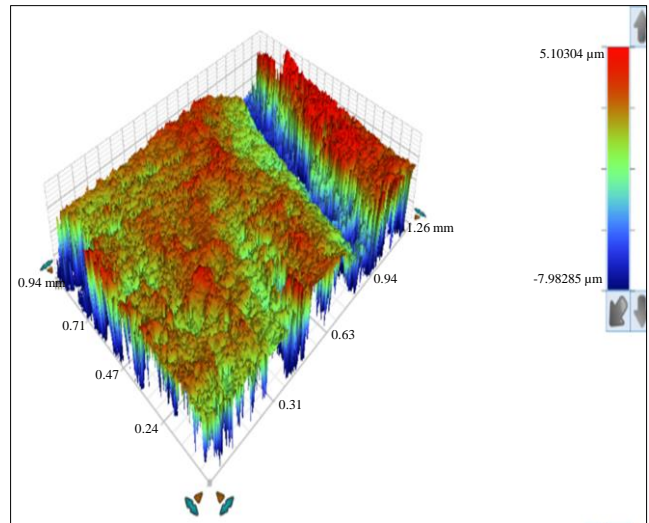


Fig. 9 Surface roughness of SIG contact post-failure (3D-sample 4)

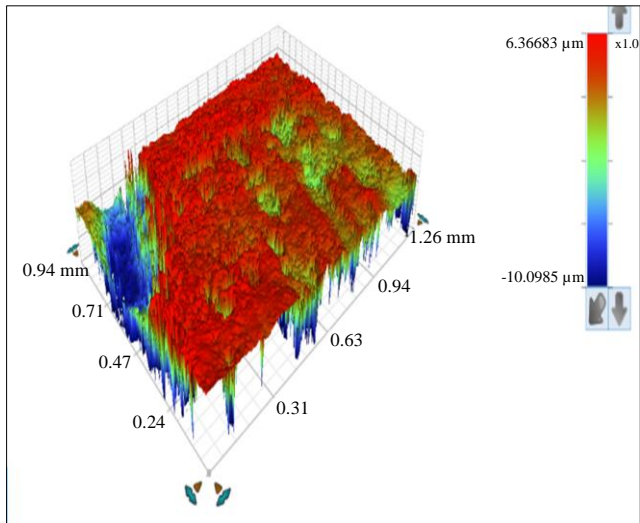


Fig. 7 Surface roughness of SIG contact post-failure (3D-sample 3)

3.1.2. FESEM Analysis

The FESEM is employed to investigate the surface topography of contacts. It displays the images at various magnifications. Figure 10 shows the movable SIG contact surface of the relay under FESEM investigation at distinct levels of magnification.

Similarly, Figure 11 shows the SIG contact surface morphology of failed SIG contact under FESEM inquiry at different magnifications. Figure 10(a) shows dismantled SIG contact using a 64MP rear phone camera.

Figures 10(b), 10(c), and 10(d) show SIG contact surface under FESEM investigation of 500μm, 50μm, and 40μm magnification before failure. Similarly, Figures 11(a), 11(b), and 11(c) show SIG contact surface under FESEM investigation of 50μm, 40μm, 2μm, and 500nm magnification after failure.

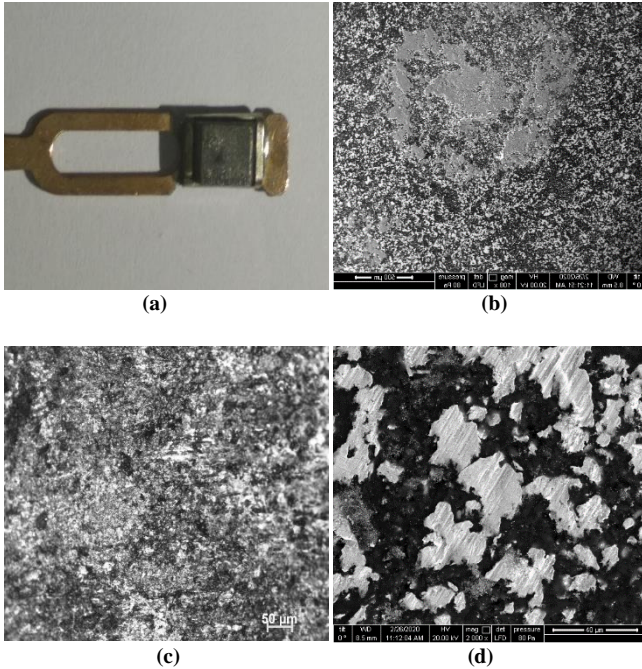


Fig. 10 FESEM image of the surface of SIG contact before failure (a) Dismantled SIG movable contact, (b) 500µm, (c) 50µm, and (d) 40µm.

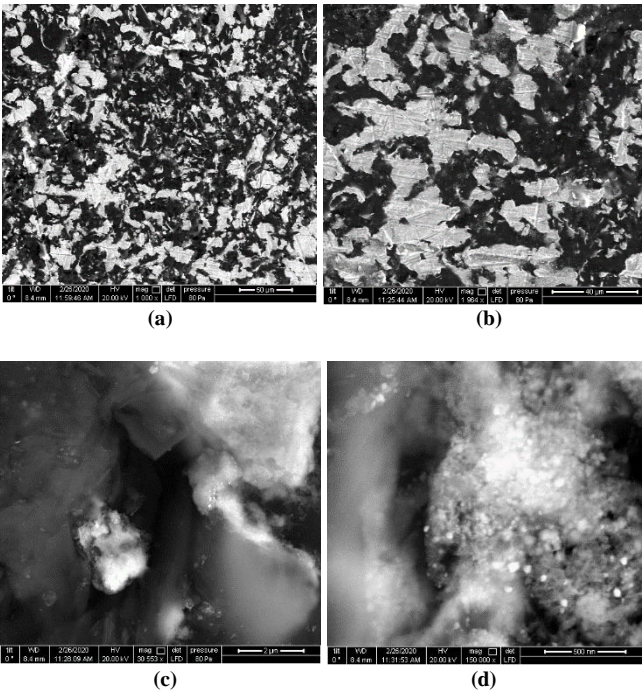


Fig 11. FESEM image of the surface of SIG contact after failure (a) SIG contact surface at 50 µm, (b) 40 µm, (c) 2 µm, and (d) 500 nm.

In Figure 10, the SIG contact of the relay before failure shows a nearly smooth surface. Movable SIG contact material is made of graphite, which is softer than fixed silver contact material. Load, stress, and environmental stress conditions affected the contact surface of the movable SIG contact. Figure 11 shows the rough surface of the contact due to

erosion, arching, and molten signs present on the surface of the SIG contact. The surface of the contact became porous, and molten metallic particles were present on the micrograph. A thin film has formed due to dirt, debris, impurities on the surface or due to oxidation, sulphation, or corrosion. Figures 11(c), and 11(d) show molten lumps and adhesion on the surface.

3.1.3. SEM Analysis

The SEM is applied to examine the surface morphology of different samples of the SIG contact. Figure 12, Figure 13, Figure 14, and Figure 15. (Sample A, Sample B, Sample C, Sample D) show various types of surface failure. Figure 12, SIG (Sample A) clearly shows contact adhesion occurred, and the surface became porous; holes and dust particles are visible in Figures 12(a), and 12(b). In Figures 12(c), and 12(d) magnified 100 µm and 50 µm images show micro-cracks and micro protrusion due to contact pressure, surface irregularities and material properties. Contact surfaces exhibit massive heat, which causes micro protrusion and micro cracks. various mechanical damage erosion, cracks, and holes are visible on the surface of the contact.

Irregularities present in the surface of the SIG contact surface (Sample B) are shown in Figure 13. Cavities and molten particles are observed on the SIG contact surface of movable contact in Figures 13(a), 13(b), and 13(c). Electrical arcing generates excessive heat. The heat vaporizes the contact material and erodes, leaving behind cavities and molten particles on the surface of the contact. The contact material gradually erodes over time due to electrical current and mechanical stress, causing holes to develop. Dust and contaminant particles caused localized corrosion or erosion, which contributed to hole formation. In Figure 13(d), a molten particle is shown. In Figures 14(a), and 14(b) molten particle particles appeared on the SIG contact (Sample C) surface due to intense electrical arcing during switching operations.

In Figure 14(d), magnified dust, dirt, and other contaminants were found on the surface of the relay contact, which caused localized areas of increased resistance. A thin film has formed on the surface of SIG contact. In Figure 15 (Sample D), a porous scalable surface is shown. Cavity, molten particles clearly visible in Figures 15(a), 15(b), 15(c), and 15(d) shows dust particles.

3.2. EDS Analysis

EDS analysis is used to assess the elemental composition of relay contact surfaces, employing X-rays to identify and quantify elements for quality control and reliability assessment. EDS analysis was performed for both moveable SIG contacts and fixed silver contacts. Figure 16 shows the spectral energy distribution of the element present on the surface of the SIG contact. The approximation of silver contact under EDS is shown in Figure 17. The mass percentage and atomic percentage of SIG contact and silver

contact are depicted in Table 2, and Table 3. From the results, SIG contact before failure had no free carbon granules present on the surface. Oxygen content was less in fresh SIG. The silver content was present in fresh SIG. Fixed silver contact before failure content silver, carbon, oxygen, and silver.

Similarly, EDS delivers energy spectrum for SIG spectrum and silver contact after failure. In Figure 18, and Figure 19 the energy spectrum of SIG contact and silver contact are shown. It is observed from Table 4 that oxidation, sulphation, and carbide formation happen, which causes high contact resistance on the SIG contact after failure. Besides other chemical impurities viz silicon dioxide, potassium oxide, zinc oxide, and calcium carbonate are present on the surface of the SIG contact.

Hence, Table 5 shows that after the failure of silver contact, silver content decreased from 85.01% to 77.15% in the failed sample. This suggested that the silver element had eroded after failure. A thin film develops on the SIG contact surface due to repeated contact cycling in relay operations. This film, in turn, triggers electrical arcing between the silver and SIG contacts, resulting in higher contact surface temperature.

The SIG contact, being softer than the silver contact, undergoes dislodgment of graphite material due to the persistent impact from more challenging silver contact during relay operation. From EDS analysis, it is observed that in addition to chemical impurities, the Sig contact surface may also accumulate contaminants such as atmospheric dust, silicon particles, sediment, and oil.

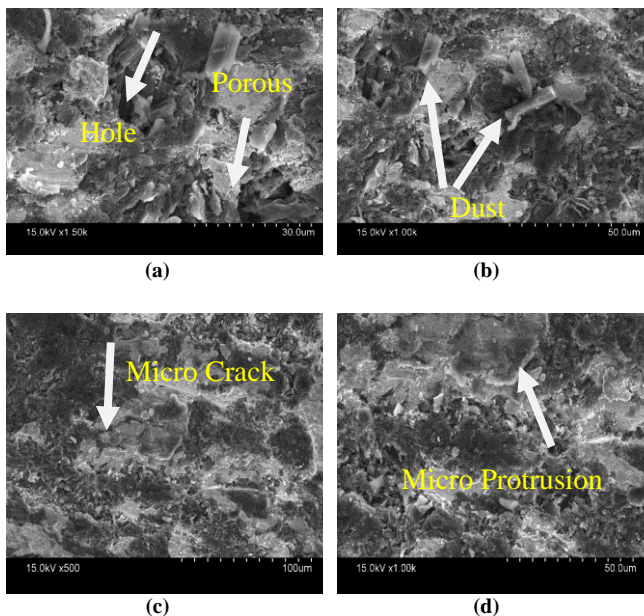


Fig. 12 SEM image of the surface of SIG contact (Sample A) after failure (a) SIG contact surface at 30 μm, (b) 50 μm (c) 100 μm, and (d) 50 μm.

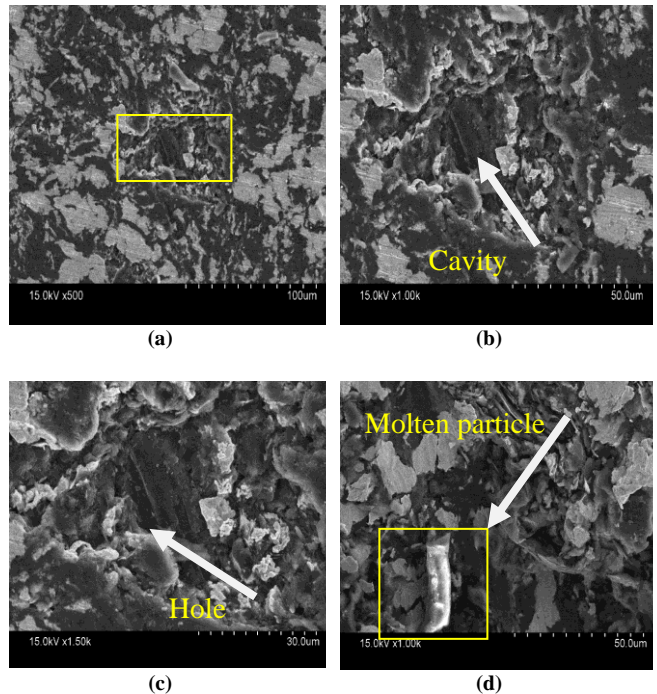


Fig. 13 SEM image of the surface of SIG contact (Sample B) after failure (a) SIG contact surface at 30 μm, (b) 50 μm (c) 100 μm, and (d) 50 μm.

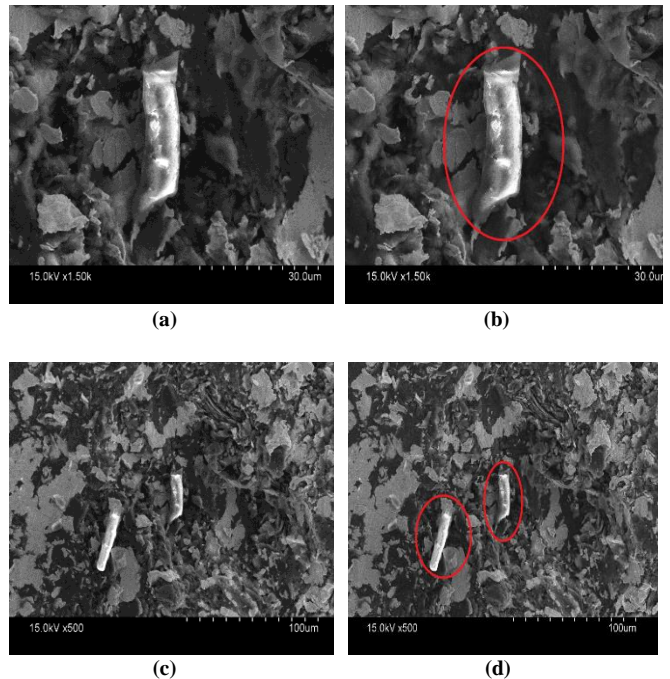


Fig. 14 SEM image of the surface of SIG contact (Sample C) after failure (a) SIG contact surface at 30 μm, (b) 50 μm (c) 100 μm, and (d) 50 μm.

Contaminants may arise from relay outgassing and catalytic effects during organic vapour decomposition in the presence of electrical arcs. These substances combine under high temperatures and arcing, leading to the formation of a

complex carbon film on the SIG contact surface. This film thickness and growth rate depend on graphite material properties, surrounding atmosphere, temperature, and duration.

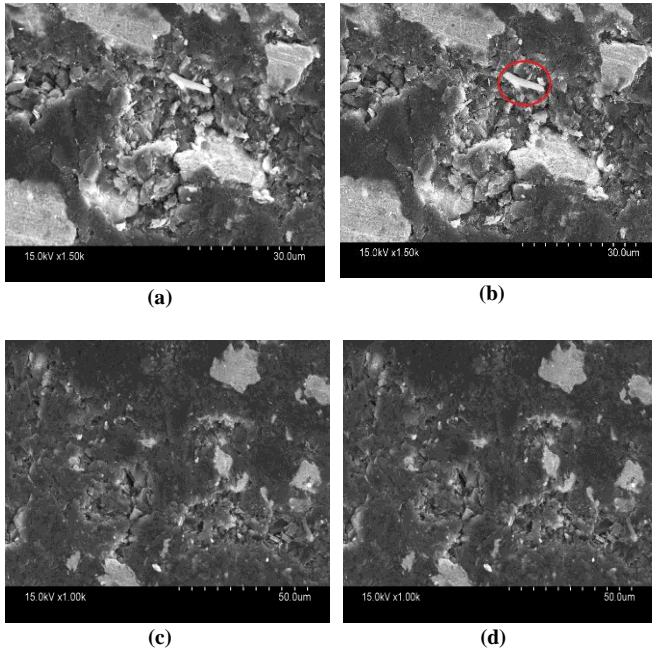


Fig. 15 SEM image of the surface of SIG contact(Sample D) after failure (a) SIG contact surface at 30 μm, (b) 30 μm (c) 30 μm, and (d) 50 μm.

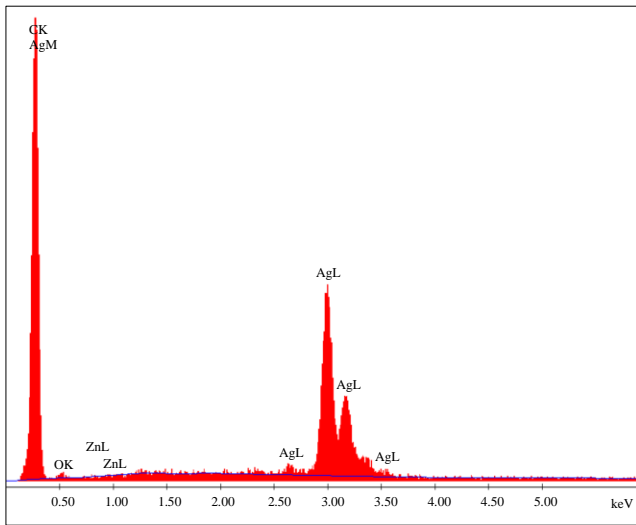


Fig. 16 EDS image of the surface of SIG contact before failure

Table 2. EDS of silver contact before failure

Element	Weight (%)	Atomic (%)
CK	8.80	39.47
OK	5.09	17.15
ZnL	1.10	0.91
AgL	85.01	42.47

Table 3. EDS of SIG contact before failure

Element	Weight (%)	Atomic (%)
CK	51.92	88.29
OK	2.40	3.06
AgL	45.69	8.65

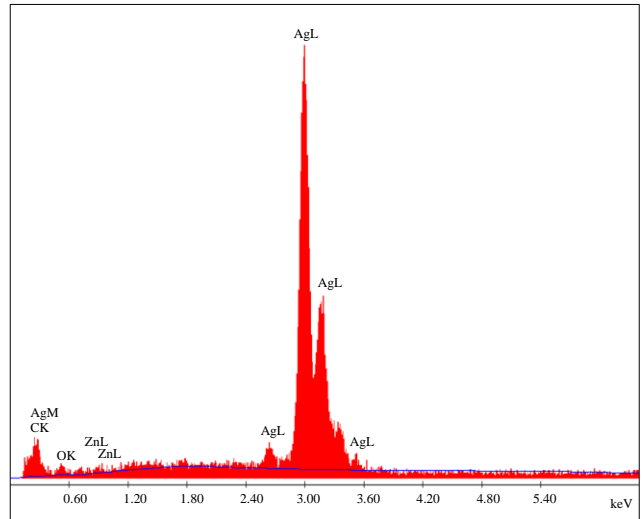


Fig. 17 EDS image of the surface of silver fixed contact before failure

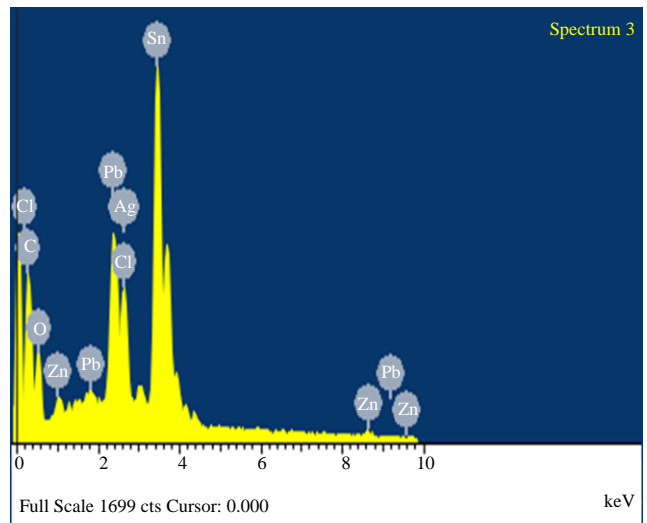


Fig. 18 EDAX image of the surface of SIG contact after failure

Table 4. EDS of SIG contact after failure

Element	Weight (%)	Atomic (%)
CK	13.99	45.75
OK	10.97	26.93
ClK	5.12	5.67
ZnL	2.11	1.27
AgL	1.63	0.59
SnL	51.22	16.95
PbM	14.96	2.84

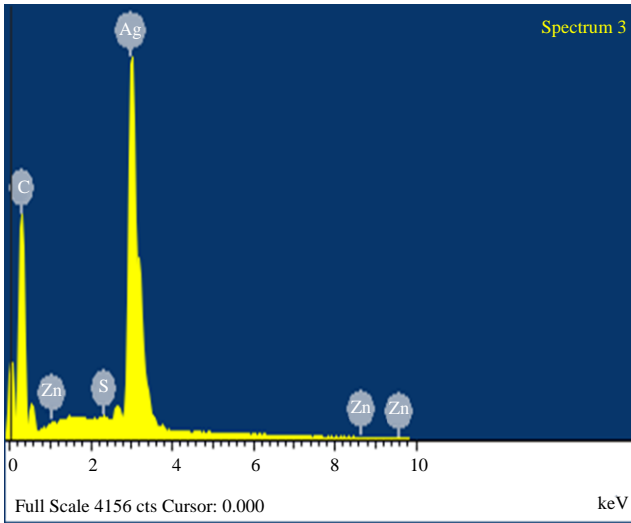


Fig. 19 EDAX image of the surface of silver contact after failure

Table 5. EDS of silver contact after failure

Element	Weight (%)	Atomic (%)
CK	22.27	71.79
SK	0.29	0.35
ZnL	0.29	0.17
AgL	77.15	27.69

Table 6. Roughness parameter for SIG contact before knocking and after 10000-knocking

Label Average	Value before Knocking	Value after 10000 Knocking
Ra	0.513 μm	1.12 μm
Rp	4.762 μm	6.367 μm
Rq	0.701 μm	1.651 μm
Rt	10.387 μm	16.465 μm
Rv	-5.625 μm	-10.098 μm

Table 7. Roughness parameter for SIG contact before knocking and after 15,000-knocking

Label Average	Value before Knocking	Value after 15,000 Knocking
Ra	0.526 μm	0.978 μm
Rp	3.537 μm	6.367 μm
Rq	0.676 μm	1.421 μm
Rt	10.822 μm	13.086 μm
Rv	-7.285 μm	-7.983 μm

Here, FESEM and SEM showed mechanical imperfections on the interaction surface of the SIG contacts. FESEM has magnified sample images in the 200 nm range. Mechanical damages are clearly visible. FESEM & SEM images were thoroughly recorded at various spectra, ranging from 2 μm , 30 μm , 40 μm , 50 μm , 100 μm , and 200nm, to offer

a comprehensive view of the various mechanical damages viz. surface irregularities, molten particles, holes, micro crack, micro protrusion, corrosion, cavities, dust, etc. EDS analysis represents the chemical composition of the element at mechanical destruction. EDS analysis also shows that oxidation, carbide formation, and sulphation on the surface of the contact erode contact material. Resulting in high contact resistance failure.

To enhance the reliability of electromagnetic relays, it is essential to prioritize regular maintenance, prevent manufacturing damage, and choose materials resistant to structural changes; compound composites or layered material may be introduced for coating. Roughness parameters have been calculated for fresh SIG contact, and roughness parameters have been calculated after 10,000 and 15,000 thousand knocking. Surface parameters have been calculated using Equation no. (1), (2), (3), (4), and (5).

Surface parameters of fresh SIG contact before knocking were as follows: Ra = 0.314, Rp = 4.829, Rq = 0.413, Rt = 9.209 and Rv = -4.38. After 10,000 knockings, the SIG surface roughness parameters are as follows: Ra = 1.12, Rp = 6.367, Rq = 1.651, Rt = 16.465, and Rv = -10.098. Another sample fresh SIG contact before knocking were as follows, Ra = 0.526, Rp = 3.537, Rq = 0.676, Rt = 10.822 and Rv = -7.285, and after 15,000 knocking SIG contact surface parameters are as follows: Ra = 0.978, Rp = 6.367, Rq = 1.421, Rt = 13.086 and Rv = -7.983.

Failed SIG contact after 10,000 and 15,000 knocking top layers roughness parameters are compared with fresh SIG here. Average roughness and profile depth have shown adhesion occurred at the relay contact.

4. Conclusion

In this work, failure analysis has been conducted on both stationary and moving relay contact surfaces. Failure analysis has been done for SIG contact under pre- and post-failure conditions. The goal was to investigate the microscopic factors contributing to the failure mechanism in metal-to-carbon relays, focusing on examining mechanical imperfections to determine the root causes of the failure. To support the context described above, surface roughness, FESEM, SEM, and EDS were conducted.

Roughness parameters have shown mechanical damages occurred after 10,000 and 15,000 knocking with respect to fresh SIG contact before knocking. Repetitive surface knocking poses a significant risk of causing severe mechanical damage, particularly when exposed to environmental stress conditions. The ongoing impact and friction contribute to accelerated wear and tear. Profilometric images vividly illustrate the extent of the mechanical damages, emphasizing the need for proactive solutions.

The moveable outer layer of the relay, when influenced by environmental factors such as moisture, dust, and excessive eating due to sparking roughness, becomes enhanced from standard unexposed contact. The anatomy of relay contact using FESEM, SEM, EDS analysis on moving contact, and EDS on stationary contact surfaces was conducted. Failure analysis has been done for SIG contact under antecedent and subsequent defective conditions. FESEM micrograph white region electron beam gathered more information concerning the black region.

SEM findings reveal that mechanical damage is attributed to melting cues and decomposition on the interface region. Airborne Oxygen in the atmosphere speeds up the oxidation process, and the generation of sulphide and carbides due to atmospheric exposure indicates contact material corrosion and erosion. EDS result proves the material chemical constitution of the element found on the interface. A thin film formed on the surface due to dust particles, debris, and impurities due to oxidation, sulphation, and corrosion. A thin film has low conductivity.

References

- [1] Zhou Zhijie et al., "Failure Prognosis Method Based on Evidential Reasoning for Aerospace Relay," *Journal of Shandong University (Engineering Science)*, vol. 47, no. 5, pp. 22-29, 2017. [[CrossRef](#)] [[Google Scholar](#)] [[Publisher Link](#)]
- [2] Guo-Fei Yu et al., "Contact Pressure of High-Voltage DC Power Relay Change and Life Prediction and Structure Optimization," *Advances in Mechanical Engineering*, vol. 13, no. 2, 2021. [[Google Scholar](#)] [[Publisher Link](#)]
- [3] Hemant Kagra, "Design of Experiment for Factors Affecting Contact Resistance in Metal to Carbon Relays," *International Journal of Science, Engineering and Technology Research*, vol. 2, no. 1, pp. 140-144, 2013. [[Publisher Link](#)]
- [4] Sun Yong-kui et al., "Failure Mechanisms Discrimination and Life Prediction of Safety Relay," *Journal of Traffic and Transportation Engineering*, vol. 18, no. 3, pp. 138-147, 2018. [[CrossRef](#)] [[Google Scholar](#)] [[Publisher Link](#)]
- [5] Jacek Mocki, and Ljubo Vlacic, "Railway Interlocking Process-Building A Base for Formal Methods," *2013 IEEE International Conference on Intelligent Rail Transportation Proceedings*, Beijing, China, pp. 146-153, 2013. [[CrossRef](#)] [[Google Scholar](#)] [[Publisher Link](#)]
- [6] Andrew J. Wileman, and Suresh Perinpanayagam, "A Prognostic Framework for Electromagnetic Relay Contacts," *European Conference of the Prognostics and Health Management Society*, vol. 2, no. 1, pp. 1-7, 2014. [[CrossRef](#)] [[Google Scholar](#)] [[Publisher Link](#)]
- [7] Hemant Kagra, and Samsul Ekram, "Contact Resistance Analysis of Silver Impregnated Graphite Contacts Used in Metal to Carbon Relays," *International Journal of Advances in Engineering Science and Technology*, vol. 2, no. 1, pp. 41-46, 2013.
- [8] Bohus Leitner, "A General Model for Railway Systems Risks Risk Assessment with the Use of Railway Accident Scenarios Analysis," *Procedia Engineering*, vol. 187, pp. 150-159, 2017. [[CrossRef](#)] [[Google Scholar](#)] [[Publisher Link](#)]
- [9] Bo Wan et al., "Failure Analysis of the Electromagnetic Relay Contacts," *Engineering Failure Analysis*, vol. 59, pp. 304-313, 2016. [[CrossRef](#)] [[Google Scholar](#)] [[Publisher Link](#)]
- [10] Cong Wang, and Nam-Young Kim, "Electrical Characterization and Nanoscale Surface Morphology of Optimized Ti/Al/Ta/Au Ohmic Contact for AlGaIn/GaN HEMT," *Nanoscale Research Letters*, vol. 7, pp. 1-8, 2012. [[CrossRef](#)] [[Google Scholar](#)] [[Publisher Link](#)]
- [11] Cheng Gao et al., "Failure Analysis for Electromagnetic Relay Contacts Adhesion by Using XES," *2014 Prognostics and System Health Management Conference (PHM-2014 Hunan)*, Zhangjiajie, China, pp. 97-101, 2014. [[CrossRef](#)] [[Google Scholar](#)] [[Publisher Link](#)]
- [12] Wang Zhaobin et al., "Storage Degradation Testing and Life Prediction for Missile Electromagnetic Relay," *Journal of Beijing University of Aeronautics and Astronautics*, vol. 42, no. 12, pp. 2610-2619, 2016. [[CrossRef](#)] [[Google Scholar](#)] [[Publisher Link](#)]
- [13] Chao Zhang, Wanbin Ren, and Tengyu Wang, "Modeling and Experimental Verification of Contact Sliding Behavior for Flexible Spring Components within Electromechanical Relays," *IEEE Transactions on Components, Packaging and Manufacturing Technology*, vol. 9, no. 10, pp. 2046-2054, 2019. [[CrossRef](#)] [[Google Scholar](#)] [[Publisher Link](#)]
- [14] Xu Zhang et al., "Effect of Electrical Load on Contact Welding Failure of Silver Tin Oxide Material Used in DC Electromechanical Relays," *IEEE Access*, vol. 7, pp. 133079-133089, 2019. [[CrossRef](#)] [[Google Scholar](#)] [[Publisher Link](#)]
- [15] Xiaohui Zhang et al., "Arc Erosion Behavior of the Al₂O₃-Cu/(W,Cr) Electrical Contacts," *Composites Part B: Engineering*, vol. 160, pp. 110-118, 2019. [[CrossRef](#)] [[Google Scholar](#)] [[Publisher Link](#)]
- [16] D. Gonzalez et al., "Model Switch Experiments for Determining the Evolution of Contact Resistance of Electrical Contacts in Contactors," *2016 IEEE 62nd Holm Conference on Electrical Contacts (Holm)*, USA, pp. 129-134, 2016. [[CrossRef](#)] [[Google Scholar](#)] [[Publisher Link](#)]
- [17] Diego Gonzalez et al., "Investigation on Contact Resistance Behavior of Switching Contacts Using a Newly Developed Model Switch," *IEEE Transactions on Components, Packaging and Manufacturing Technology*, vol. 8, no. 6, pp. 939-949, 2018. [[CrossRef](#)] [[Google Scholar](#)] [[Publisher Link](#)]
- [18] V. Behrens et al., "Analytical Methods to Identify Root Causes for Early Failure of an AC Contactor with Heavy Load Service Life Test," *2019 IEEE Holm Conference on Electrical Contacts*, USA, pp. 303-308, 2019. [[CrossRef](#)] [[Google Scholar](#)] [[Publisher Link](#)]
- [19] Nachiketa Ray et al., "Effect of WC Particle Size and Ag Volume Fraction on Electrical Contact Resistance and Thermal Conductivity of Ag-WC Contact Materials," *Materials & Design*, vol. 85, pp. 412-422, 2015. [[CrossRef](#)] [[Google Scholar](#)] [[Publisher Link](#)]

- [20] Salisu Nasir et al., "Carbon-Based Nanomaterials/Allotropes: A Glimpse of their Synthesis, Properties and Some Applications," *Materials*, vol. 11, no. 2, pp. 1-24, 2018. [[CrossRef](#)] [[Google Scholar](#)] [[Publisher Link](#)]
- [21] Femi Robert, "Investigation on Graphene-Coated Silver-Palladium Microelectrical Contact and Effect of Coating Thickness," *IEEE Transactions on Components, Packaging and Manufacturing Technology*, vol. 10, no. 11, pp. 1821-1828, 2020. [[CrossRef](#)] [[Google Scholar](#)] [[Publisher Link](#)]
- [22] Femi Robert et al., "Investigation of Graphene as a Material for Electrical Contacts in the Application of Microrelays Using Finite Element Modeling," *Materials Research Express*, vol. 6, no. 9, 2019. [[CrossRef](#)] [[Google Scholar](#)] [[Publisher Link](#)]
- [23] Guanyu Cao et al., "Contrastive Research on Electrical Contact Performance for Contact Materials of Cu-SnO₂ and Cu-ZnO₂ Alloys," *Materials Research*, vol. 22, no. 3, pp. 1-7, 2019. [[CrossRef](#)] [[Google Scholar](#)] [[Publisher Link](#)]
- [24] Wenhua Li et al., "Research on Contact Difference Plane Layering and Corrosion Zoning of Sealed Relay Contacts," *IEEJ Transactions Electrical and Electronic Engineering*, vol. 14, no. 11, pp. 1595-1601, 2019. [[CrossRef](#)] [[Google Scholar](#)] [[Publisher Link](#)]
- [25] S. Biyika, and M. Aydin, "Investigation of the Effect of Different Current Loads on the Arc-Erosion Performance of Electrical Contacts," *Acta Physica Polonica A*, vol. 129, no. 4, pp. 656-660, 2015. [[Google Scholar](#)]
- [26] Stephen D. Campbell, "Evaluation of Surface Roughness and Polishing Techniques for New Ceramic Materials," *The Journal of Prosthetic Dentistry*, vol. 61, no. 5, pp. 563-568, 1989. [[CrossRef](#)] [[Google Scholar](#)] [[Publisher Link](#)]
- [27] Bulem Yuzugullu et al., "The Effects of Extraoral Porcelain Polishing Sequences on Surface Roughness and Color of Feldspathic Porcelain," *International Journal of Prosthodontics*, vol. 22, no. 5, pp. 472-475, 2009. [[Google Scholar](#)] [[Publisher Link](#)]
- [28] Z. Pavlovic, D. Risovic, and D. Novakovic, "Comparative Study of Direct and Indirect Image-Based Profilometry in Characterization of Surface Roughness," *Surface and Interface Analysis*, vol. 44, no. 7, pp. 825-830, 2012. [[CrossRef](#)] [[Google Scholar](#)] [[Publisher Link](#)]